Single to quadruple ionization of CO_2 due to electron impact

Cechan Tian and C. R. Vidal
Max-Planck-Institut für Extraterrestrische Physik, P.O. Box 1603, 85740 Garching, Germany
(Received 18 June 1998)

The electron-impact multiple ionization and the subsequent dissociation of CO_2 have been studied for electron energies from the threshold to 600 eV. The dissociation channels of up to quadruply ionized carbon dioxide molecules have been identified. The absolute cross sections for the ion-pair dissociation channels in double, triple, and quadruple ionization of CO_2 have been obtained. The absolute cross sections of the other channels involving neutral fragments are also derived. The experiment shows that the total cross section of single, double, and triple ionization decreases by at least an order of magnitude as the ionization stage increases by 1. By studying the structure of the islands in the covariance maps, we have concluded that one of the ${CO_2}^{2+}$ dissociation channels ${CO_2}^{2+} \rightarrow C^+ + O^+ + O$ is dominated by the process of secondary decay. The dissociation channel ${CO_2}^{2+} \rightarrow 2O^+ + C$ is a concerted process. The three-body dissociation channels of triply ionized carbon dioxide are found to be dominated by concerted processes no matter how the charges are distributed on the fragments. The momentum distribution on the fragments can only be explained by the charge mobility during the dissociation process of the triply ionized molecules. The metastable decay of ${CO_2}^{2+}$ is also observed directly. [S1050-2947(98)08911-2]

PACS number(s): 34.80.Gs, 34.50.Gb

I. INTRODUCTION

The structure and the dissociation dynamics of multiply ionized molecules have attracted growing interest in recent years [1]. Different excitation sources such as high-intensity lasers [2,3], heavy particle beams [4,5], synchrotron radiation [6–9] and electron beams [10,11] have been applied to remove electrons from the valence or inner shells of the molecules. The electric field strength produced by high-intensity laser beams is at the same level or even higher than the internal Coulomb field of the molecules. The electronic states of the molecules are dressed with the laser field, resulting in complex ionization and dissociation dynamics. Heavy particle collisions have been shown to be very powerful in exciting molecules into high ionization stages. The molecules tend to ''explode'' because of the strong internal Coulomb field. This has resulted in the term ''Coulomb explosion.'' Under the interaction of synchrotron radiation or electron impact, molecules are usually ionized to lower stages. However, the tunable excitation energy of these sources allows one to study the dissociation dynamics near the threshold and at relatively low energies.

In the present paper we report the investigation of the multiple ionization of carbon dioxide due to electron impact. The electron gun has the advantage of cheap and easy construction. This is one of the reasons why it has been adopted in experiments for a long time. After the multiple ionization of CO_2, experiments have shown that some molecules are stable and some others are metastable [17]. However, a very significant fraction of the ionized molecules will dissociate into different branches consisting of two or three fragments. In the dissociation channels consisting of two fragments, the two parts carry the same momenta and the dissociation dynamics is more straightforward. However, the dissociation dynamics for the channel consisting of three fragments is more complex. The three fragments can also be formed in a single step, i.e., the molecule explodes directly into three fragments, or they are formed in two successive steps, i.e., the molecule dissociates in the first step into two fragments, where one of them is metastable, which then dissociates further into two other fragments. The location of the charge on the intermediate and the final fragments also complicates the dissociation dynamics. The study of the three-body dissociation has resulted in the terms of sequential and concerted mechanisms [12,13]. Sequential mechanisms are further categorized as secondary decay and deferred charge separation according to the charge location. The concerted mechanisms are divided into synchronous or asynchronous according to the time difference in the fragment formation.

In the present work we study the electron impact multiple ionization and the dissociation dynamics of CO_2 with a covariance mapping mass spectroscopic technique. The covariance mapping technique has proven to be very powerful in studying the dissociation dynamics of molecules [10,12,13]. We report the measurements for the cross sections of different dissociation channels and the study of the dissociation dynamics. The dissociation of multiply ionized CO_2 has been studied by Frasinski *et al.* [3] with high intensity lasers, by Masuoka *et al.* [9] with synchrotron radiation and by Matsuo *et al.* [14] with heavy particle collisions. The present work reports the absolute cross sections and dissociation dynamics of different dissociation channels of multiply ionized CO_2 due to electron impact.

II. EXPERIMENT

A. Dissociation channels after multiple ionization of CO_2

The possible dissociation channels after the multiple ionization of CO_2 are listed in Table I. Since no triply charged ions have been observed experimentally [17], the channels related to their production have been neglected. The corresponding dissociation limits were calculated based on the data for the dissociation energies and ionization potentials from Herzberg [15] and Moore [16]. In this table we list

TABLE I. The different dissociation channels after the multiple ionization of CO_2. For an explanation of *a*–*d* see the text.

Parent ion	C^{2+}	O^{2+}	C^+	O^+	CO_2^{2+}	CO^+	CO_2^+	C	O	(C,O)	(O,O)	Dissociation limit (eV)
$CO_2^+ \rightarrow$							CO_2^+					stable[a]
						CO^+			O			19.467[d]
				O^+						(C,O)		19.067[d]
			C^+								(O,O)	27.822[d]
$CO_2^{2+} \rightarrow$					CO_2^{2+}							metastable[a]
			C^+	O^+					O			41.432[b]
				$2O^+$				C				43.782[b]
				O^+		CO^+						33.081[b]
	C^{2+}										(O,O)	51.198[d]
		O^{2+}								(C,O)		54.213[d]
$CO_2^{3+} \rightarrow$	C^{2+}			O^+					O			64.808[b]
		O^{2+}		O^+				C				78.928[b]
		O^{2+}	C^+						O			76.578[b]
		O^{2+}				CO^+						68.227[b]
			C^+	$2O^+$								67.158[c]
$CO_2^{4+} \rightarrow$	C^{2+}	O^{2+}							O			100.026[b]
	C^{2+}			$2O^+$								90.534[c]
		O^{2+}	C^+	O^+								103.304[c]

identical products in the same column, so that we clearly see which channels contribute to the total production of the corresponding fragments. The symbol (C, O), for example, means that the products can either be two separate atoms, C and O, or a CO molecule. To measure the cross section for each channel, we distinguish four types, denoted with *a*, *b*, *c*, and *d* in Table I. In the channels denoted with *a* no dissociation occurs. The cross section for them can therefore be measured in a conventional way [17]. The channels marked with *b* consist of an ion pair with or without a neutral fragment. The channels marked with *c* correspond to the dissociation of the molecules into three ionic fragments. For measuring the cross sections of channels denoted with *b* and *c*, the ions must be detected selectively in a unique way. Hence, coincidence techniques have to be used. The channels marked with *d* consist of an ion and some neutral fragments. If we check Table I, we find that each subcolumn of the second column consists of at most only one *d* channel. Since we know the total cross section for each ionic product [17], we can readily derive the absolute cross sections of all *d*-type channels if we have determined the cross sections for *b*- and *c*-type channels.

B. Experimental setup for the cross-section measurements

In order to measure the cross sections for *b*- and *c*-type dissociation channels, the ions must be measured by coincidence techniques. The experimental setup is shown schematically in Fig. 1. The experimental setup consists of a molecular beam crossed with an electron beam, and a focusing time-of-flight mass spectrometer, which has already been described in detail [17,18]. Briefly, a cw effusive molecular beam is crossed with a pulsed electron beam (100 nsec) at right angles. The molecular beam is produced by a gas flow from a long needle with a diameter of 0.4 mm passing through a skimmer. The top of the needle is about 2 cm above the skimmer and the skimmer is about 6 cm above the electron beam. The interaction region is less than 4 mm×4 mm× 4 mm. About 100 nsec after the decay of the electron beam a pulsed voltage is applied to the extraction mesh of the mass spectrometer. The ions are extracted into a specially designed focusing time-of-flight (FTOF) mass

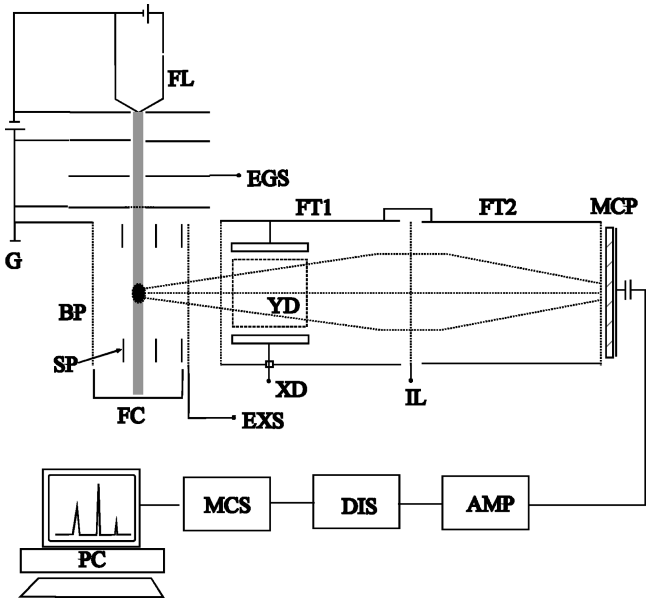

FIG. 1. Experimental setup. FL, filament; EGS, electron gun switch; FC, Faraday cup; G, ground; BP, backing plate; SP, shield plate; EXS, ion extraction switch; YD, Y deflector; XD, *X* deflector; FT1, flight tube 1; FT2, flight tube 2; IL, ion lens; MCP, microchannel plate; AMP, amplifier; CFD, constant fraction discriminator; MCS, mulitchannel scaler; PC, personal computer.

spectrometer [17]. The shield plates in the interaction region of the FTOF mass spectrometer make the extraction mesh to a plane-convex lens, which focuses the ions close to the axis of the FTOF mass spectrometer when the ions leave the ion source region. It also reduces the divergence angle with respect to that in the extraction system of a normal Wiley-McLaren TOF mass spectrometer. The flight tube of the FTOF mass spectrometer is segmented into two sections of identical length with a fine mesh in between. The fine mesh performs as a spherically symmetric lens if the voltage applied to it is about 1.3–1.4 times the voltage on the flight tubes. The detection plane is thus the image of the acceleration plane. In order to make the system more efficient in collecting the energetic ions produced by the dissociation of multiply ionized molecules, the voltages on the extraction mesh, flight tubes, and the focusing lens are raised compared to the previous work. In the experiments the voltage applied to the extraction mesh is typically -0.85 kV, that on the flight tubes is -1.75 kV, and that on the focusing mesh is -2.33 kV.

As described in detail in a previous publication [17], the focusing effect of the present time-of-flight mass spectrometer raises significantly the tolerance of the detection system with respect to the initial kinetic energy and the starting position of the ions. Ion trajectory calculations show that with the present voltage settings the ions with an initial kinetic energy of as high as 25 eV/charge can be collected with the same efficiency as the thermal ions in the focusing time-of-flight mass spectrometer. The kinetic energy release in the dissociation of the doubly ionized CO_2 has been measured by Masuoka *et al.* [9], which are well within the collection capability of the present setup. For triple and quadruple ionization, no data on the kinetic energy release exist. The kinetic energy release of triple and quadruple ionization of CO due to the fast ion beam collisions was measured by Mathur *et al.* [5] and Sampoll *et al.* [4]. If the kinetic energy of the fragments from the electron impact ionization of CO_2 is similar to that from CO due to a fast ion beam (although most probably it is smaller), we assume that all the ionic fragments from triple ionization and more than 90% of the ions from quadruple ionization can be collected by the present setup.

C. Experimental setup for dissociation dynamics

For the study of the dissociation dynamics, we replace the FTOF with a normal Wiley-McLaren time-of-flight mass spectrometer, which is called TOF2. The electron gun and the effusive molecular beam are identical with those in the cross-section measurements with the FTOF. In this TOF2 the electric field in the interaction region and that in the flight tube are homogeneous so that the dissociation dynamics can be more easily interpreted. The lengths of the interaction region, acceleration region, and the flight tube are 12 mm, 14 mm, and 425 mm, respectively. The detector and the electronics are identical with those used in the previous cross-section measurement with the FTOF. The voltage on the flight tubes is adjustable from 1 to 2 kV, and that on the extraction mesh is also adjusted correspondingly.

D. Covariance mapping mass spectroscopy of CO_2

Another major difference of the present experiment from the previous work is the coincidence technique. For the selective and exclusive detection of the products from multiple ionization of the molecules, the ionic fragments have to be detected in coincidence. Here we measure the cross sections of these channels and investigate the dissociation dynamics by studying the covariance mapping mass spectroscopy of the fragments [3,19]. The technique of covariance mapping mass spectroscopy was developed by Frasinski *et al.* [3,19]. In this technique the autocorrelation function of each single-shot spectrum is calculated and accumulated. After a long time accumulation the coincidence spectra are illustrated in a two-dimensional map as shown in Fig. 2. A normal time-of-flight mass spectrum is also shown on the X as well as in Y axis of Fig. 2. Every count on the two-dimensional map corresponds to the detection of an ion pair. If the total number of counts in each single shot is very small, the accumulated spectrum can be used to determine the cross sections for the ion pairs as described by Frasinski *et al.* The structure of each island is actually a momentum contour, which can be used to interpret the dynamics in the dissociation process. At the top of Fig. 2 there is a line that consists of several islands, where every count corresponds to the detection of a CO_2^+ and a further ion. Physically it is not possible to produce a CO_2^+ as well as another ion from a single CO_2 molecule. Hence, these counts must originate from false coincidences, where the ions are produced from different molecules. In order to subtract the false coincidence counts, a spectrum accumulated from single-count events is also recorded at the same time, which is used to subtract the false coincidence in a similar way to that of Bruce *et al.* [10]. Briefly, the autocorrelation function of the single-count spec-

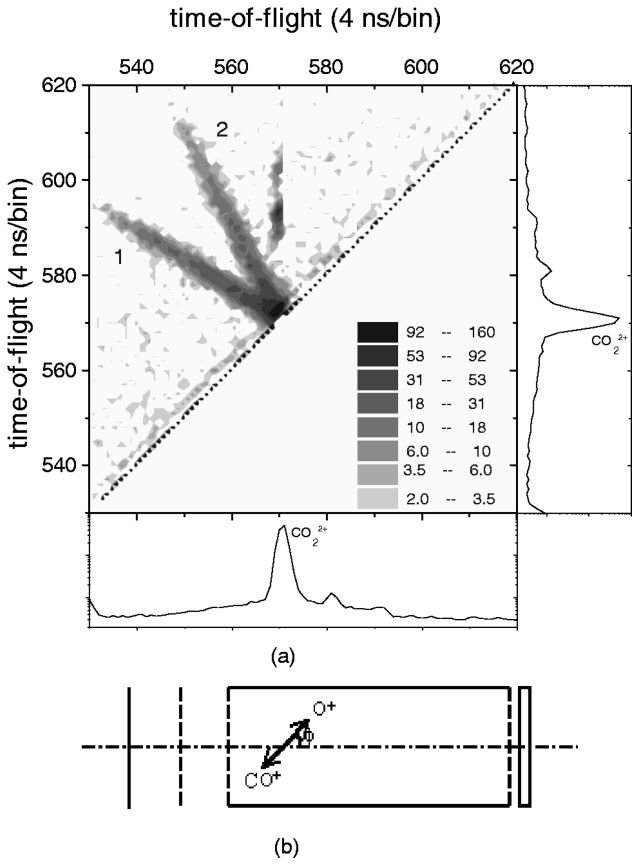

FIG. 2. Covariance mapping mass spectrum of CO_2 at the electron energy of 600 eV, raw data.

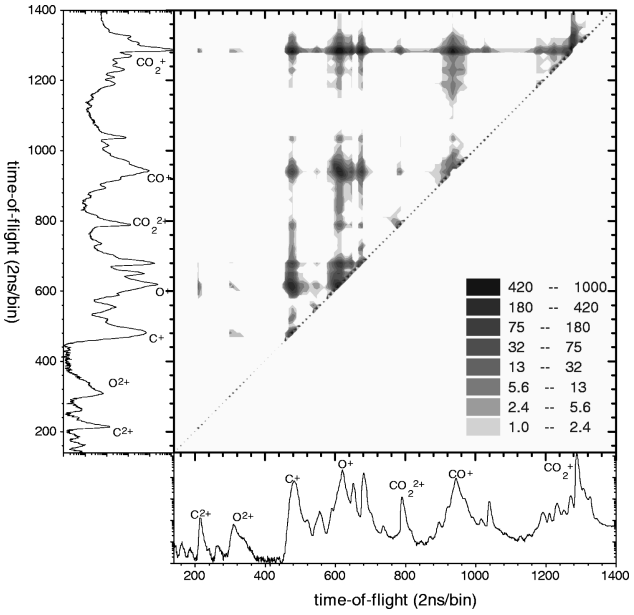

FIG. 3. Covariance mapping mass spectrum of CO_2 at the electron energy of 600 eV, after the subtraction of the false coincidence.

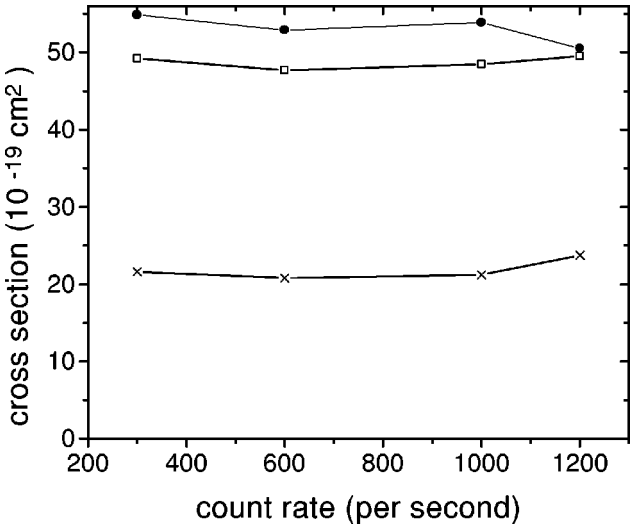

FIG. 4. The dependence on the count rate for the cross sections of CO_2^{2+} dissociative channels at the electron energy of 600 eV. $C^+ + CO^+$ (-●-), $C^+ + O^+ + O$ (-□-), $2O^+ + C$ (-×-).

trum is calculated, and the amplitude of the islands corresponding to the detection of a pair of CO_2^+ and another ion is normalized to that in the accumulated covariance map. Then it is subtracted from the covariance map. The covariance mapping mass spectrum after the removal of the false coincidence is shown in Fig. 3. After the subtraction we see that some statistically insignificant fluctuation around 0 is left at the top of the map.

The absolute cross section of an ion pair, for instance $C^+ + O^+$, is obtained by

$$\sigma(C^+ + O^+) = \frac{n_{\text{coincidence}}}{n_{\text{total}} T \eta} \sigma(\text{total}), \tag{1}$$

where n_{total} is the total number of ions. σ(total) is the total ionization cross section of CO_2 [17]. T is the total transmission of the meshes in the time-of-flight mass spectrometer. η is the detection efficiency of the microchannel plate. We get the transmission of the meshes from the measurement of the optical transparency and the open area from the manufacturer's manual [20]. The two data agree with each other. We get $T = 58.1\%$. For the detection efficiency of the microchannel plate, we use the open area ratio from the manufacturer's manual, which is 60% [21]. It has been proven experimentally by a number of authors that the detection efficiency of the microchannel plate is equal to its physically open area ratio [22–25].

Here we want to note that for the products of a channel consisting of an ion pair and a third fragment, we always get the total cross sections of the channels in which the third fragment is either neutral or charged. If the third fragment is charged, this channel is a *c*-type channel. The measurement of the cross section for these channels requires in principle a triple coincidence, i.e., a three-dimensional covariance mapping technique, which has not been done in the present work. However, since a charged third fragment always corresponds to a higher order of ionization, its cross section is expected to be smaller than the channel with a neutral third fragment by at least an order of magnitude. As a result, we consider that what we get from Eq. (1) is the cross section of the channel with a neutral third fragment. For getting the data at a particular electron energy, the accumulation takes 2 h at a repetition rate of 5 kHz. Usually the measurements have been repeated at least four times. The statistics are taken to get the final cross-section values and the data fluctuations.

E. Error estimate in the cross-section measurements

A very important error source in the measurement of *b*-type channels is due to the false coincidence. In order to verify how much the false coincidence contributes in the present work, we measured the cross sections of *c*- type channels at different count rates by adjusting the molecular density and the electron beam current. The count rates for the true coincidence are proportional to the molecular density and the electron beam current, whereas the count rates of the false coincidence are proportional to the squares of the molecular density and the electron beam current. The results on the ion-pairs of $C^+ + O^+$, $O^+ + CO^+$, and $O^+ + O^+$ are shown in Fig. 4. We can see that the data fluctuate within $\pm 4\%$ although the total count rate has increased from 300 to 1200/sec. This suggests that our subtraction of the false coincidence is very effective. The false coincidence thus does not cause a large error in our measurements. Further error sources can be due to the error of the total cross section data of CO_2 (15%), those of the absolute transmission of all the meshes and that of the detection efficiency of the microchannel plate. As a result, we expect that the total error of the measurements for the channel with an ion pair is about 20%. For the channels with an ion pair and a neutral fragment, the cross section may be overestimated because we cannot distinguish whether the third fragment is neutral or charged. The error is expected to be about 25%. Because of the diagonal noise and the dead channels of the discriminator and the mutlichannel scaler, the error for the channels with $2O^+$ is

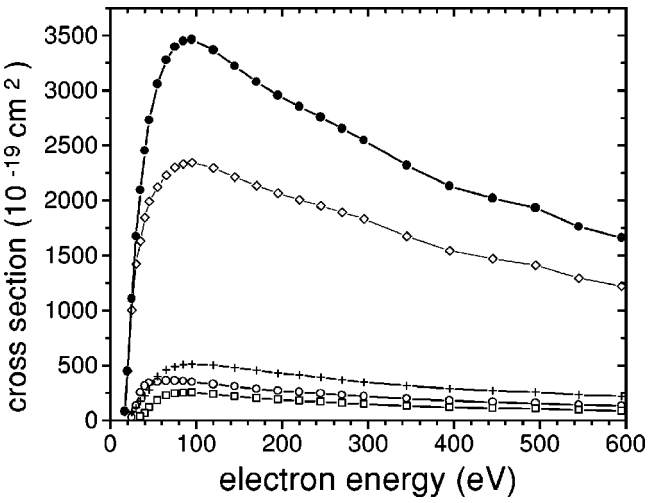

FIG. 5. The cross sections of the possible dissociation channels after single ionization of CO_2. The products are CO_2^+ (-◇-), $CO^+ + O$ (-○-), $O^+ + (C, O)$ (-+-), and $C^+ + (O, O)$ (-□-). The total cross section of the single ionization is shown by -●-.

larger. We expect that it is about 25%. We subtracted the diagonal noise and made the compensation to the dead channels assuming that the peak of the island $O^+ + O^+$ is flat near the diagonal of the covariance map. For the *d*-type channels, the cross section is derived indirectly. Since we neglected the *c*-type channels, the error is expected to be about 25%.

III. RESULTS AND DISCUSSION

A. Cross sections and dissociation ratios

The cross sections of the four possible channels after the single ionization of CO_2 (as listed in Table I) are shown in Fig. 5. The values for the three dissociative channels are listed in Table II. That for CO_2^+ has been published before [17], so it is not included in Table II. The total cross section for single ionization is obtained by summing the cross sections of the four channels. We can see that the maximum of the total cross section for the single ionization is at about 90 eV. The dominant channel is the formation of the stable CO_2^+. The cross sections of three dissociative channels $CO_2^+ \rightarrow CO^+ + O$, $CO_2^+ \rightarrow O^+ + (C, O)$ and $CO_2^+ \rightarrow C^+ + (O,O)$ are relatively small. Locht and Davister studied the dissociation channels of CO_2^+ for the electron energies between 19 and 40 eV. They found that at high electron energies, the ionic fragments originate exclusively from the multiple electron transition states of CO_2^+. These multiple electron transition states are probably all unstable in all three dissociative channels. If this is true, the stable CO_2^+ ions should be populated into single electron transition states and most likely at low energies. Even at high electron energies, the transition is still dominated by single electron transitions to lower bound states of CO_2^+. At high electron energies, the channel $CO_2^+ \rightarrow O^+ + (C, O)$ has the highest cross section among the three dissociation channels.

The cross sections for the six possible channels after a double ionization, which are also listed in Table I, are shown

TABLE II. The cross sections (10^{-19} cm^2) of different dissociation channels after single and double ionization of CO_2.

	Single ionization			Double ionization				
EE	$CO^+ + O$	$O^+ + (C, O)$	$C^+ + (O, O)$	$O^+ + CO^+$	$2O^+ + C$	$C^+ + O^+ + O$	$O^{2+} + (C, O)$	$C^{2+} + (O, O)$
595	132	218	87.5	53.8	21.1	48.4	0.376	0.0341
545	141	233	94.2	58.4	22.7	52.7	0.526	0.115
495	155	256	105	65.8	25.0	59.1	0.598	0.206
445	164	271	111	71.4	27.2	64.3	0.506	0.456
395	177	290	119	76.4	30.0	71.5	0.711	0.396
345	197	318	132	85.4	34.7	80.7	0.775	0.594
295	218	349	149	98.4	39.1	92.2	0.893	0.720
270	231	370	160	103	41.8	99.4	0.952	0.841
245	245	392	169	107	43.8	104	0.923	1.00
220	255	410	178	114	46.0	109	1.08	1.13
195	270	430	188	121	46.7	113	1.08	1.36
170	284	455	203	126	47.1	113	1.12	1.39
145	308	481	218	129	45.2	109	1.07	1.50
120	329	503	238	130	38.9	94.9	0.926	1.23
95	350	513	252	120	26.2	66.1	0.527	0.857
85	356	507	251	110	20.6	53.4	0.285	0.562
75	360	488	245	96.5	14.2	36.9	0.138	0.255
65	359	460	226	73.8	10.2	20.3		
55	349	400	183	44.1	7.56	7.68		
45	340	277	120	13.8	3.46	1.52		
40	314	222	68.1					
35	252	175	35.0					
30	136	116						
25	28.4	75.2						

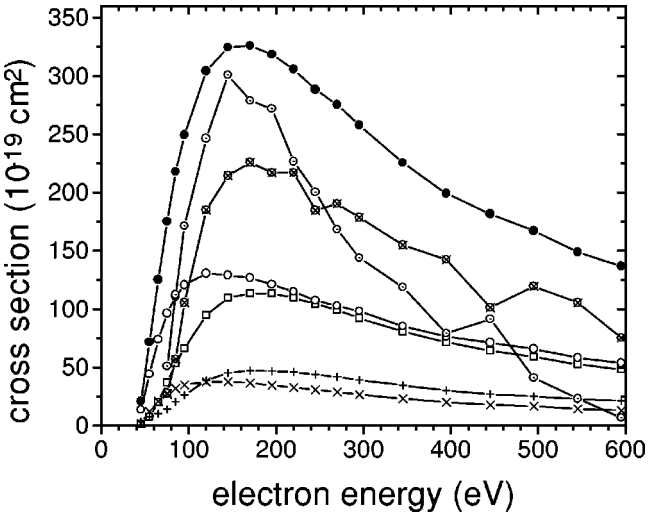

FIG. 6. The cross sections of the possible reaction channels after double ionization of CO_2. The products are CO_2^{2+} (-×-), $C^+ + O^+ + O$ (-□-), $CO^+ + O^+$ (-○-), $O^+ + O^+ + C$ (-+-) $(C^{2+} + (O, O)) \times 200$ (-⊙-), and $[(C, O) + O^{2+}] \times 200$ (-⊗-). The total cross section of double ionization is shown by -●-.

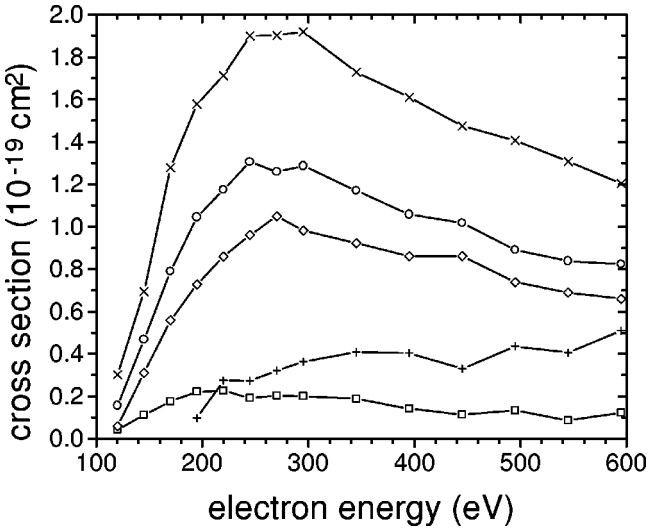

FIG. 7. The cross sections of the channels $O^{2+} + CO^+$ (-□-), $O^+ + O^{2+} + C$ (-○-), and $(O^{2+} + C^+ + O)$ (-◇-), $C^{2+} + O^+ + O$(-×-) after triple ionization of CO_2. Also the cross section of a dissociation channel of quadruple ionized CO_2: $(C^{2+} + O^{2+} + O) \times 10$ $(- + -)$ is shown.

in Fig. 6. The results for the five dissociative channels are listed in Table II. In the first channel metastable CO_2^{2+} molecules are produced and the cross sections can be measured directly with the conventional techniques [17]. The three channels with ion pairs are measured with the present covariance mapping mass spectroscopic techniques. The cross sections for the other two channels, which are multiplied by a factor of 200 in Fig. 6, are derived from the data obtained in the last step. The maximum for the total double ionization cross section lies at an electron energy of 160 eV, which is higher than that of the single ionization by about 70 eV because the electronic states of the doubly ionized carbon dioxide should lie at a higher energy range than those of the singly ionized molecules. The total cross section for double ionization is also about 10 times lower than that for single ionization. Instead of the formation of stable CO_2^{2+}, the dominant channel after the double ionization is the equal charge two body separation process $CO_2^{2+} \rightarrow O^+ + CO^+$. However, the cross sections for the channels of CO_2^{2+} and $CO_2^{2+} \rightarrow O^+ + CO^+$ maximize at the same electron energy of 120 eV, suggesting that these two channels may involve similar electronic states of CO_2^{2+}. The cross sections of the channels of $CO_2^{2+} \rightarrow C^+ + O^+ + O$ and $CO_2^+ \rightarrow 2O^+ + C$ have very different shapes compared with the two channels mentioned above. They maximize at the electron energy of 170 eV, which is much higher than that of the other two channels. This suggests that the dissociation of the channels of $CO_2^{2+} \rightarrow C^+ + O^+ + O$ and $CO_2^{2+} \rightarrow 2O^+ + C$ may involve very different electronic states from that of the channel $CO_2^{2+} \rightarrow O^+ + CO^+$. This will be studied later in the analysis of the dissociation dynamics. It is very improbable that the two charges concentrate on a single atom after the double ionization of CO_2. As a result the cross sections of the channels $CO_2^{2+} \rightarrow O^{2+} + (C, O)$ and $CO_2^{2+} \rightarrow C^{2+} + (O, O)$ are smaller than those of the previous channels by a factor of at least 50.

Among all the dissociation channels after the triple ionization of carbon dioxide, the dominant one should be due to the equal charge separation channel $CO_2^{3+} \rightarrow 2O^+ + C^+$. However, the measurement of the cross section for this channel requires triple coincidence techniques, which has not been available in the present work. The results for the measured channels are shown in Fig. 7 and are listed in Table III. We can see that no stable CO_2^{3+} is observed in the experiment. The carbon dioxide molecules tend to dissociate into the smallest possible fragments after triple ionization. Hence the cross section for the two-body separation channel $CO_2^{3+} \rightarrow O^{2+} + CO^+$ is the smallest among all the measured channels. The maximum of the cross section for this channel lies at about 200 eV, whereas that for the other channels lies at about 270 eV. These energies are much higher than those for the single and double ionization because the electronic states of the triply ionized carbon dioxide lie at higher energies. The total cross section of the measured channels is more than two orders of magnitude lower than that for double ionization. If all the channels are measured, the total cross section is still expected to be smaller than that for double ionization by at least an order of magnitude.

Among all the channels after the quadruple ionization of carbon dioxide, we can only measure the cross sections for the channel $CO_2^{4+} \rightarrow C^{2+} + O^{2+} + O$, which are also shown in Fig. 7 and listed in Table III. For clarity, the result is multiplied by a factor of 10 in Fig. 7. We see that the cross sections for this channel are lower than those for the triple ionization channels by at least one order of magnitude. The cross section maximizes at even higher electron energies.

The dissociation ratios for single and double ionization of CO_2 are shown in Fig. 8. We see that at the electron energies above 300 eV, the dissociation ratios almost reach constant values at 26% and 90% of the single and double ionization, respectively. For triple and quadruple ionization, the dissociation ratios are both 100%. This indicates that after the single ionization of CO_2, most of the molecules stabilize into some electronic states of CO_2^+. However, after higher stages of ionization, the Coulomb interaction inside the mol-

TABLE III. The cross sections (10^{-19} cm^2) of different dissociation channels after triple and quadruple ionization of CO_2.

	Triple ionization				Quadruple
EE	$O^{2+}+C^{+}+O$	$O^{2+}+O^{+}+C$	$O^{2+}+CO^{+}$	$C^{2+}+O^{+}+O$	$C^{2+}+O^{2+}+O$
595	0.660	0.823	0.122	1.20	0.051
545	0.689	0.838	0.0866	1.30	0.041
495	0.738	0.890	0.133	1.40	0.044
445	0.862	1.01	0.113	1.47	0.033
395	0.862	1.05	0.142	1.61	0.040
345	0.922	1.17	0.188	1.72	0.041
295	0.981	1.28	0.200	1.91	0.036
270	1.04	1.25	0.202	1.90	0.032
245	0.960	1.30	0.191	1.90	0.027
220	0.859	1.17	0.226	1.71	0.027
195	0.727	1.04	0.221	1.57	0.01
170	0.559	0.788	0.174	1.27	
145	0.310	0.467	0.113	0.693	
120	0.0591	0.156	0.0422	0.303	

ecules is so large that the atoms tend to fly apart. Hogreve [26] calculated the lowest electronic states of CO_2^{2+}, and found that the ground-state potential energy surface has a local minimum with a potential barrier larger than 1 eV for a collinear symmetric configuration. This potential barrier keeps the molecules metastable after double ionization and results in the experimentally observed CO_2^{2+}. However, most of the CO_2^{2+} molecules cannot remain stable. Hence they dissociate into different fragments. For triply and quadruply ionized carbon dioxide, the Coulomb interaction is even stronger. No local minimum on the potential surface is expected. This is the reason why no stable triply or quadruply ionized carbon dioxide molecules are observed experimentally. The dissociation ratios of CO_2 after single and double photoionization were measured by Masuoka [28]. At the photon energy of 100 eV, their results agree with the present work.

B. Dissociation dynamics

The covariance mapping mass spectroscopic technique has been demonstrated to be very powerful in studying the dissociation dynamics of multiply ionized molecules [3,10,13]. The structures of the ion pair islands are determined by the momenta carried by the corresponding ion pair. The experiment was done with the TOF2 system because the electric fields in the interaction region and the flight tube are homogeneous and the dissociation dynamics can therefore be more easily interpreted.

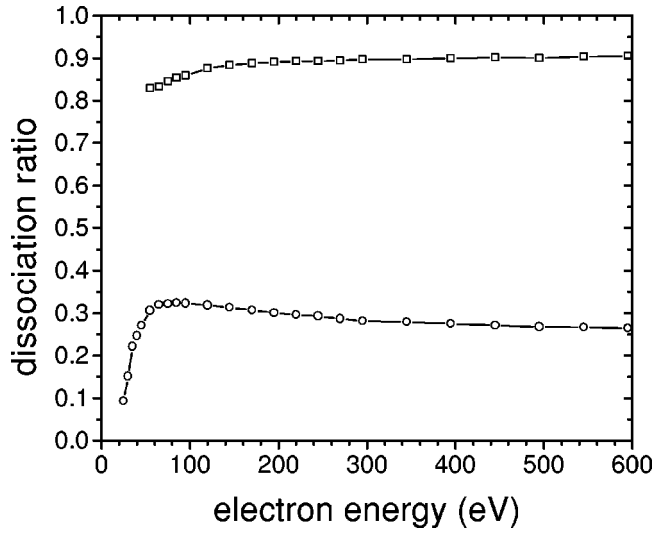

FIG. 8. The dissociation ratios after the single ($-\bigcirc-$) and double ($-\square-$) ionization of CO_2.

1. Dissociation of doubly ionized CO_2

The ion-pair islands corresponding to the dissociation of doubly ionized carbon dioxide molecules at the electron energy of 600 eV are shown in Figs. 9(a)–9(c), respectively. In the measurements the voltage on the flight tube is set to 1 kV. The streaks in Fig. 9(c), which are parallel to the diagonal axis, might originate from noise and dead channels of the constant fraction discriminator or the multichannel scaler. During the flight of the ions towards the detector, some ions may produce secondary particles when they collide with any one of the meshes in the flight path. These secondary particles always coincide with the original ions. This forms the strong line that is parallel to the *Y* axis in Fig. 9(c) and at the *X* time bin of 675. If we compare the structures of the islands, we see that the island in Fig. 9(a), which corresponds to the dissociation channel of $CO_2^{2+} \rightarrow O^{+} + CO^{+}$, has a very sharp and narrow structure. However, the island in Fig. 9(b), which corresponds to the channel $CO_2^{2+} \rightarrow O^{+} + C^{+} + O$, has a much broader structure and a different orientation. That in Fig. 9(c), which corresponds to the channel $CO_2^{2+} \rightarrow 2O^{+} + C$, has a similar orientation to that in Fig. 9(a). In the middle of each island, the numbers of counts are lower, because the counts here correspond to those molecules that dissociate when their internuclear axes are perpendicular to the axis of the TOF2. Most of the ions that initially fly in this direction are lost.

The theoretical analysis of the covariance mapping mass spectroscopy has shown that the structure of the ion-pair islands is a momentum contour. With the definition of the orientation angle θ illustrated in the lower left part of Fig. 9, we have [10]

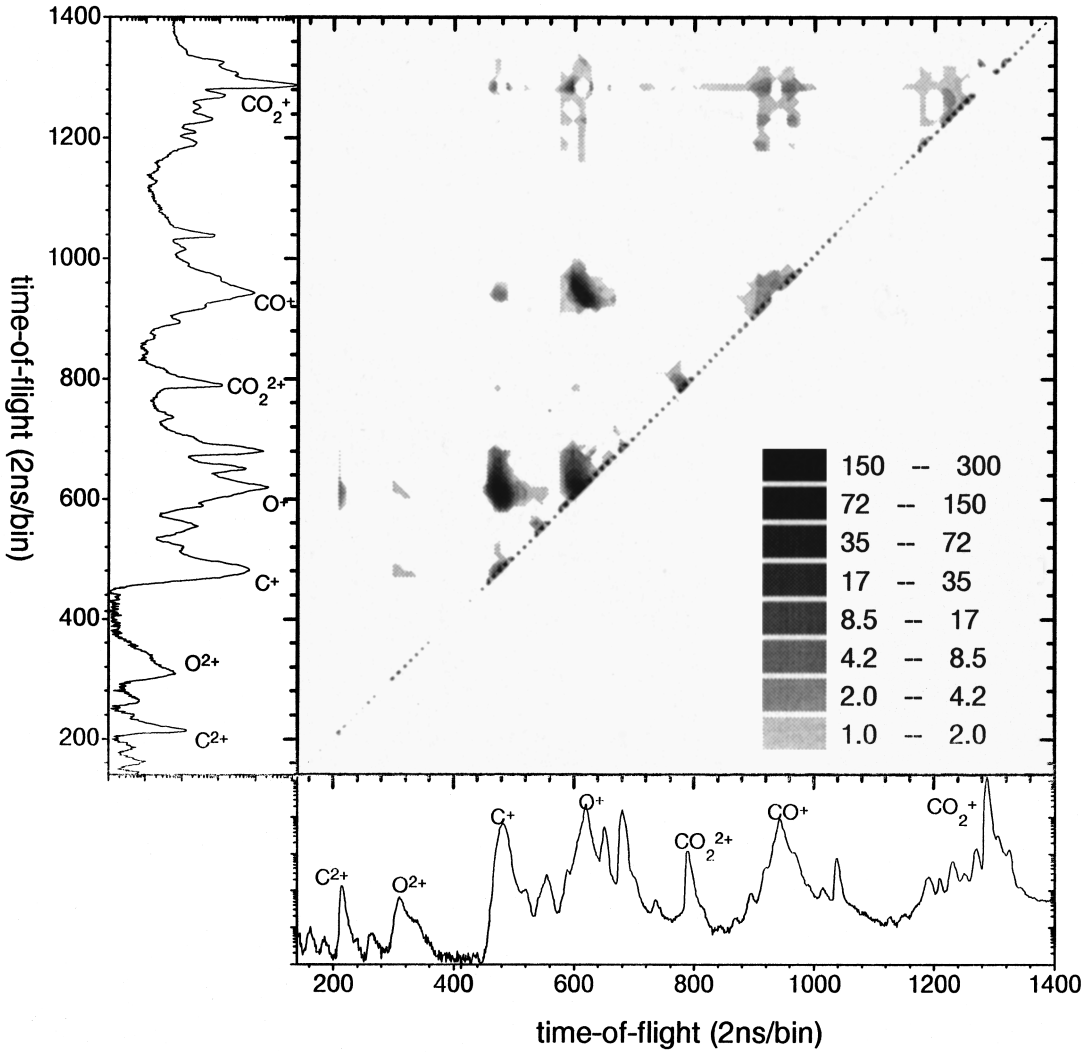

FIG. 9. The detailed structure of the ion-pair islands in the covariance mapping mass spectra. The parent ion is CO_2^{2+}. The corresponding dissociation channels are (a) $CO_2^{2+} \rightarrow O^+ + CO^+$, (b) $CO_2^{2+} \rightarrow O^+ + C^+ + O$, and (c) $CO_2^{2+} \rightarrow 2O^+ + C$, respectively. In the lower left part the definition of the orientation angle is shown.

$$\theta = \tan^{-1} \frac{P_Y}{P_X} \frac{Q_X}{Q_Y}, \tag{2}$$

where P and Q are the momentum and charge of the ions, respectively. X and Y represent the ions drawn in the X and Y direction, respectively. The dissociation channel $CO_2^{2+} \rightarrow O^+ + CO^+$ is a simple two-body separation, where the two fragments remove the same amount of momentum in opposite directions. From Eq. (2) we see that for this dissociation channel $\theta = 45°$. The angle in Fig. 9(a) is $45° \pm 1°$, which is in excellent agreement with the expectation. The island is also sharp and narrow because it is a simple two-body separation.

However, CO_2^{2+} can also dissociate into $C^+ + O^+ + O$ with different dynamics. They are described in detail in the following.

(a) Deferred charge separation:

$$CO_2^{2+} \rightarrow O + CO^{2+} \rightarrow O + C^+ + O^+. \tag{3}$$

This mechanism therefore occurs in two steps. In the first step CO_2^{2+} dissociates into two parts with different charges, O and CO^{2+}. In the second step the doubly charged fragment CO^{2+} dissociates into C^+ and O^+. As a result, in the frame of the center of mass of C^+ and O^+ the two ions carry the same amount of momenta in opposite directions. The center of mass of C^+ and O^+ carries the same momentum as the neutral fragment O but in opposite directions.

(b) Secondary decay:

$$CO_2^{2+} \rightarrow O^+ + CO^+ \rightarrow O^+ + C^+ + O. \tag{4}$$

This mechanism also occurs in two steps. In the first step CO_2^{2+} dissociates into two parts with the same charge, O^+ and CO^+. In the second step CO^+ dissociates into C^+ and O. Since O^+ and the intermediate fragment CO^+ carry the same amounts of momenta in opposite directions, in the second step CO^+ releases much less kinetic energy than in the first step, as a result, C^+ carries a fraction $m_C/(m_C + m_O)$ of the momentum on CO^+.

(c) Concerted separation:

$$CO_2^{2+} \rightarrow O^+ + C^+ + O. \tag{5}$$

This mechanism occurs in a single step, although the fragmentation of the molecules can be synchronous or asynchronous. In either case O^+ and O are expected to carry a similar amount of momentum in opposite directions. C^+ is expected to carry much less momentum than O^+ and O because it is located in the center of the linear triatomic molecule.

Since the momentum distributions on the fragments resulting from different dynamics are different, the structure of the island can be used to interpret the dissociation dynamics. The island in Fig. 9 (b) has a broad structure, but the overall angle is $70° \pm 2°$, which is very close to the angle predicted by secondary decay process, where we get $\theta = \tan^{-1}\frac{28}{12} = 66.8°$. Hence we conclude that the dissociation of CO_2^{2+} is dominated by secondary decay. The width of the island also suggests that in the second step of the decay, the intermediate fragment CO^+ releases also some amounts of kinetic energy. We also studied the same channel at low electron energies ($\leqslant 100$ eV), we get an orientation angle of $67° \pm 1°$. This is in excellent agreement with the theoretical prediction. All these suggest that at high electron energies, because higher electronic states are involved, there might be a minor contribution from concerted mechanism to the dissociation channel $CO_2^{2+} \rightarrow O^+ + C^+ + O$. Masuoka and coworkers [9] also studied this dissociation channel with photoionization. Their experiment supports the present conclusion.

It is very unlikely that the dissociation of CO_2^{2+} into $2O^+ + C$ can occur through deferred charge separation. Since the angle of the O^+-O^+ island in Fig. 9(c) is $45° \pm 2°$, we concluded that the $2O^+ + C$ fragments are formed through concerted separation of the three fragments. The two O^+ ions carry similar amounts of momentum. The dissociation channel is thus synchronous. The broader structure of this island suggests that there might be a minor asymmetry when the two O^+ ions fly away from the C atom. Hence the C atom may also carry some small amount of momentum.

2. Dissociation of triply ionized CO_2

The islands in Fig. 10 correspond to the dissociation channels of triply ionized carbon dioxide molecules. These islands have a much lower total number of counts and a poor signal-to-noise ratio, although the data were accumulated over 24 hours and the voltage on the flight tube was elevated to 2 kV to increase the collection efficiency to the fast fragments produced by the dissociation of CO_2^{3+}. However, we can still see some internal features. Four of the CO_2^{3+} dissociation channels are illustrated in Figs. 10(a) $CO_2^{3+} \rightarrow O^{2+} + CO^+$, (b) $CO_2^{3+} \rightarrow C^+ + O^{2+} + O$, (c) $CO_2^{3+} \rightarrow O^+ + O^{2+} + C$, and (d) $CO_2^{3+} \rightarrow O^+ + C^{2+} + O$, respectively. From the orientations of the islands we get the angle and the momentum ratios of the corresponding ion pairs, as listed in Table IV. The structures of the islands indicate that in all the dissociation channels of CO_2^{3+} the fragments are produced by synchronous concerted mechanism. The widths of the islands in Figs. 10(b)–10(d) suggest that the directions of the momenta carried by the fragments are slightly noncollinear. In order to explain the structures more clearly, we show the projection of the momenta on the internuclear axis in the lower left part of Fig. 10 for each corresponding dissociation channel. If we generalize the momentum carried by the fragments produced in the dissociation of triply ionized carbon dioxide molecules, we find that all the O fragments (O atom, O^+, and O^{2+}) always carry a large amount of momenta. In strong contrast to this all the C fragments (C atom, C^+, and C^{2+}) always remove much less momentum, no matter how the charges are distributed on the final fragments.

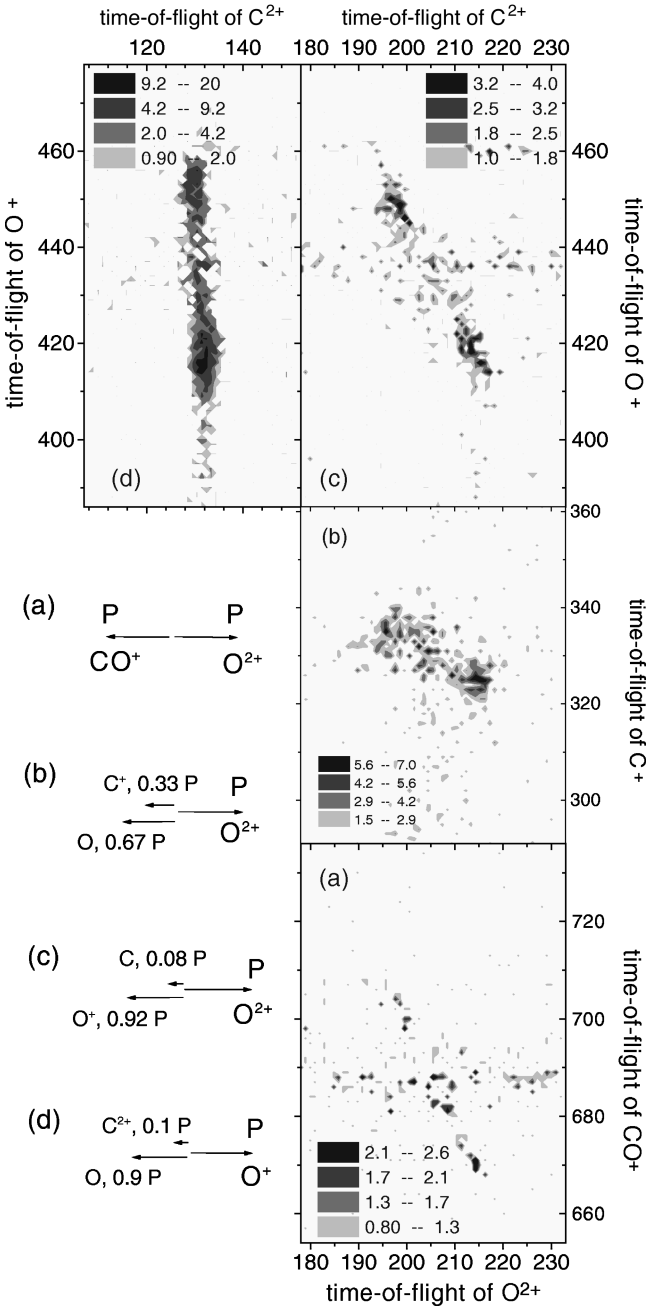

FIG. 10. The detailed structure of the ion-pair islands in the covariance mapping mass spectra. The parent ion is CO_2^{3+}. The corresponding dissociation channels are (a) $CO_2^{3+} \rightarrow O^{2+} + CO^+$, (b) $CO_2^{3+} \rightarrow O^+ + C^{2+} + O$, (c) $CO_2^{3+} \rightarrow O^+ + O^{2+} + C$, and (d) $CO_2^{3+} \rightarrow O^+ + C^{2+} + O$, respectively. In the lower left part the momentum distributions of each dissociation channel are shown.

In order to understand the charge and momentum distribution in the fragmentation of multiply charged ions, Hsieh and Eland [12] proposed a charge exchange model. In this model when a multiply charged molecule dissociates, all the

TABLE IV. The angle and momentum ratio of CO_2^{3+} dissociation channels.

Channel	$O^{2+}+CO^+$	$O^{2+}+C^++O$	$O^{2+}+O^++C$	$C^{2+}+O^++O$
Angle	$64°\pm2°$	$33.4°\pm2°$	$61.5°\pm2°$	$87°\pm1°$
Momentum ratio	$0.94<P_{CO^+}/P_{O^+}<1.12$	$0.31<P_{C^+}/P_{O^{2+}}<0.35$	$0.84<P_{O^+}/P_{O^{2+}}<1.00$	$\frac{P_{O^+}}{P_{C^{2+}}}\approx 9.5$

fragments initially share the electric charge by rapid exchange until the distance between them becomes too large. Quantum mechanically, the densely located potential surfaces cross each other. During the expansion of the molecule, the molecule frequently jumps from one state to another at the internuclear distance from 2 to 6 Å. Hence the electric charge frequently moves from one atom to another. As a result, during the dissociation all the fragments feel the effects of the Coulomb repulsion and gain momentum from the release of any unbalanced repulsion. When the distance between the fragments becomes too large for the charge mobility, the electric charges are localized on certain fragments. The Coulomb repulsion at this distance will cause some minor difference in the momentum distributions for the fragments with different final charged states. The charge exchange model of Hsieh and Eland [12] can also explain the momentum and charge distribution in the present measurements, which cannot be explained by a charge-localized model. For instance, in the dissociation channel $CO_2^{3+}\rightarrow O^+ + C^{2+} + O$ [Fig. 10(d)], the doubly charged fragment C^{2+} carries only about 10% of the momentum of O^+. However, the neutral fragment O carries 90% of the momentum of O^+. If the charges are localized as C^{2+} and O^+ from the beginning of the dissociation, the Coulomb repulsion should be mainly between C^{2+} and O^+. Since C^{2+} is located at the center of the linear configuration of CO_2, C^{2+} should remove a similar momentum as the neutral fragment O. However, this is different from the present experimental observation, which can only be explained by the charge exchange model. Channel $CO_2^{3+}\rightarrow O^+ + C^{2+} + O$ [Fig. 10(b)] is another example that can only be explained by the charge mobility during the dissociation process.

3. Direct observation of the metastable decay of CO_2^{2+}

Besides the ion-pair islands discussed above, we also observed a special structure in the vicinity of the CO_2^{2+} peak. The corresponding part of the covariance map is shown in Fig. 11(a). Next to the two-dimensional map the corresponding part of the normal mass spectrum is illustrated in *X* and *Y* directions, respectively. We can see that there are two arms in the map, labeled with 1 and 2, respectively. Arm 1 and arm 2 cross each other on the diagonal axis, where the time-bin is exactly the center of the CO_2^{2+} peak. At this bin, there is also a structure parallel to the *Y* axis, which is caused by the collision of the ions with the meshes and similar to that in Fig. 9(c). The orientation angles of arm 1 and arm 2 are $31°\pm2°$ and $62°\pm2°$, respectively. If we analyze in the same way as that for the islands in Figs. 9 and 10, the structure in Fig. 11 would correspond to the coincidence of two CO_2^{2+} ions. However, it is not possible to have such a coincidence because the backing pressure in the experiment is only about 3 torr. No dimers can be formed in the effusive flow through the long needle. Also no indication of dimers was observed in the experiment.

The structure in Fig. 11(a) can only be explained by noting the metastability of CO_2^{2+}. CO_2^{2+} molecules are known to be metastable in the collinear configuration [26]. As mentioned above, the ground electronic state has a local shallow potential well with a barrier higher than 1 eV above the dissociation limit of $O^+ + CO^+$. This potential well makes CO_2^{2+} metastable, which then dissociates after a long lifetime. Similar structures have also been observed by Field and Eland in the photoionization of the diatomic and triatomic molecules, from the structures of the two arms the authors obtained the mean lifetime of the metastable doubly charged molecules [27]. The mean lifetime for CO_2^{2+} was estimated to be around 900 ns. During the present experiment CO_2^{2+} ions are extracted into the flight tube within a duration of about 600 ns. The CO_2^{2+} ions arrive at the detector within a time duration of 4 μs. If CO_2^{2+} dissociates when it is still in the interaction region, the fragments will arrive at the detector in a time that is dependent on the masses of the fragments. However, if the dissociation occurs when CO_2^{2+} is already inside the flight tube, the fragments will have the same overall velocity as their parent ion, CO_2^{2+}. The dissociation process contributes some extra kinetic energy to the fragments, which is much smaller than that produced by the extraction and acceleration fields. As a result, the fragments will arrive at the detector in a time duration that is similar to their parent ion. The metastable decay of CO_2^{2+} is shown schematically in Fig. 11(b), where we define ϕ as the angle of the O^+ momentum in the center-of-mass frame of $O^+ + CO^+$ with respect to the flight direction. If l is the distance between the detector and the CO_2^{2+} ion when it dissociates, P is the momentum of O^+ in the center-of-mass frame, $T_{CO^{2+}}$ is the total flight time of CO_2^{2+} if it does not dissociate, v is the velocity of CO_2^{2+} in the flight tube, and M is the mass of the fragment, the flight time of O^+ is given by

$$T_{O^+}=T_{CO^{2+}}-\frac{l}{v^2}\frac{P\cos\phi}{M_{O^+}}. \tag{6}$$

Similarly, the flight time of the other fragment CO^+ is given by

$$T_{CO^+}=T_{CO^{2+}}+\frac{l}{v^2}\frac{P\cos\phi}{M_{CO^+}}. \tag{7}$$

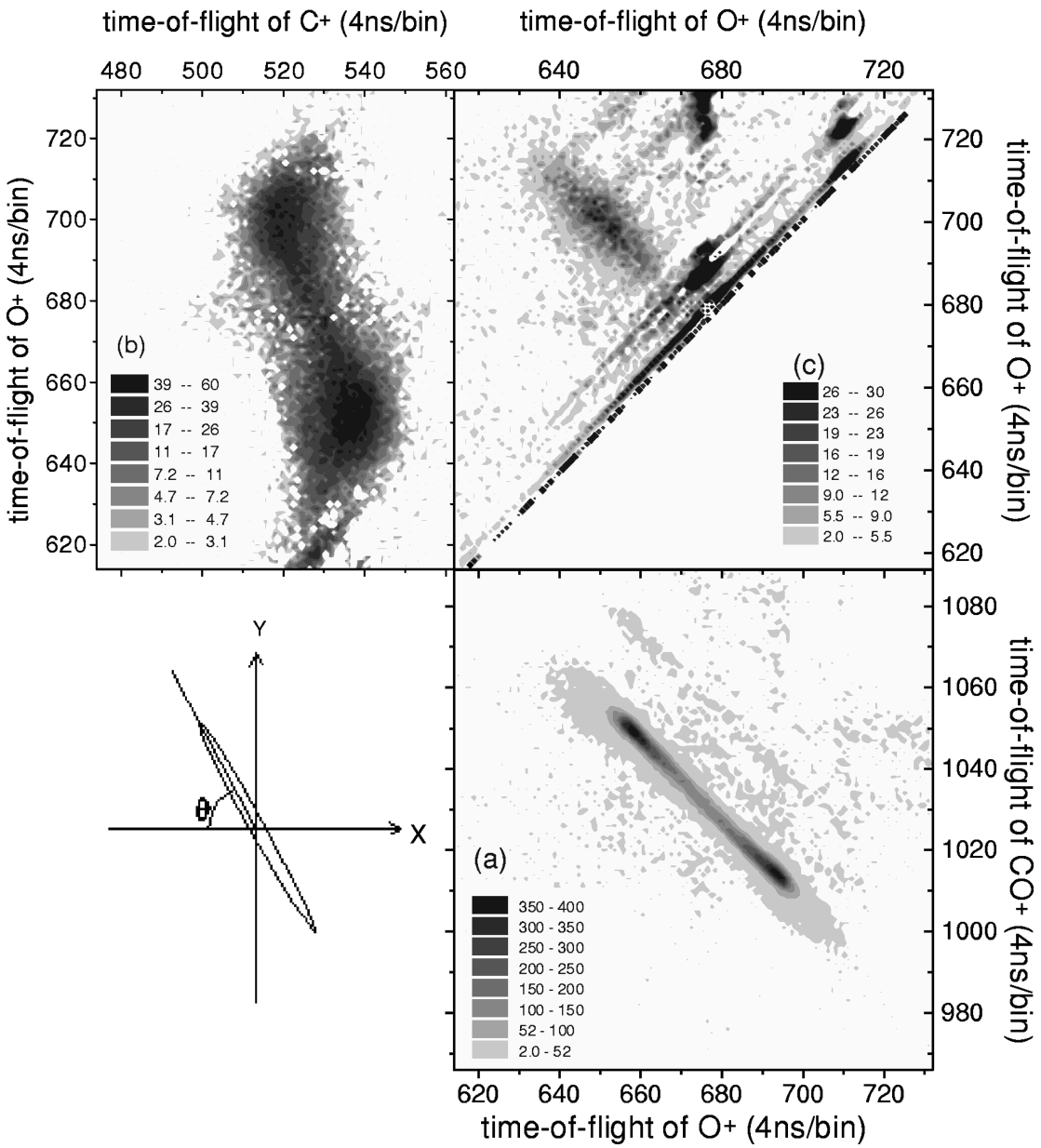

FIG. 11. (a) The structure of the covariance map in the vicinity of CO_2^{2+} peak. (b) The metastable decay of CO_2^{2+} in the flight tube is illustrated schematically.

If a dissociation occurs, we will measure a count at (T_{O^+}, T_{CO^+}). Because CO_2^{2+} can dissociate at all possible l and ϕ values. We therefore get the two arms in Fig. 11(a), where arm 1 and 2 correspond to $0°<\phi<90°$ and $90°<\phi<180°$, respectively. The orientation angles of arm 1 and 2 are thus given by $\tan^{-1}\theta_1 = M_{O^+}/M_{CO^+}$ and $\tan^{-1}\theta_2 = M_{CO^+}/M_{O^+}$, respectively. We calculated $\theta_1 = 29.7°$, and $\theta_2 = 60.2°$, which are in excellent agreement with the experiment.

From the analysis we see that the map in Fig. 11(a) is actually a velocity contour rather than a momentum contour as in Figs. 9 and 10. In a two-body dissociation, the two fragments carry the same amount of momentum and the orientation angle will directly indicate the mass ratio of the two fragments. In the experiment we did not observe any other structures, suggesting that all the electronic states corresponding to the other channels have a much shorter lifetime. The corresponding dissociations occur when the CO_2^{2+} ions are still in the interaction region.

4. Further discussion

The dissociation dynamics of CO_2 has also been studied with VUV photoionization [9], heavy-ion impact [14], and high-intensity laser fields [19]. Here we would like to compare the dynamics of these different excitation mechanisms with the present work. In the electron impact part of the electron energy is transferred to the outer- or inner-valence electron(s) of the molecules. The incident and the released electrons leave the molecules within a typical duration of $10^{-16}-10^{-17}$ s. The dissociation occurs after the decay of the interaction. In the VUV photoionization all the photon energy is transferred to the outer or inner electron(s) and the outgoing electrons remove part of the photon energy. Afterwards the other electrons rearrange themselves. The dissocia-

tion dynamics should be similar to those in electron impact excitation except that the initial electronic states might be different. In both, photoionization and electron impact, the cross section decreases by orders of magnitude as the ionization stage increases. Also the fragments carrying more than three charges have not been observed before to our knowledge. The advantage of photoionization and electron impact processes is that the excitation energy is adjustable from below threshold to quite high energies. The starting channels and the dissociation under different ionization stages can therefore be studied in detail. Heavy ion impact has been observed to be much more efficient in ionizing molecules. Fragments with charges as high as 6 have been observed. The reason is because a heavy ion can transfer more energy to the molecules. The experiment also shows that the atom located at the center of the molecule usually carries more positive charges. The cross sections have also been observed to decrease as the ionization stage increases, although not as rapidly as those in photoionization and electron impact ionization. The interaction time for heavy ion impact is similar to that for electron impact. The dissociation also happens after the decay of the interaction field. Intense laser field ionization involves very different ionization and dissociation dynamics from the former three processes. The major difference is that the interaction time in intense laser field ionization is the same as the laser pulse duration, which is much longer than that in electron impact, heavy ion impact, and photoionization processes. The laser field generates dressed states inside the molecules. Hence the ionization and dissociation involve complex dynamics, which has not yet been understood. Experiments show that the kinetic energy release is usually smaller than what is expected in the Coulomb explosion model. The cross section also does not necessarily decrease as the ionization stages increase. Frasinski *et al.* [3] found that the sixth order of ionization is most probable in the multiphoton ionization of CO_2 at their laser intensity. The models of laser-induced trapping and stabilization have been introduced to understand the abnormal kinetic energy release and abundance of the ionic fragments [29,30].

IV. CONCLUSIONS

The multiple ionization of molecules and its dissociation dynamics have recently attracted much interest. In the present paper we have investigated the multiple ionization and the subsequent dissociation of CO_2 with an electron beam for electron energies up to 600 eV. Dissociation channels up to quadruply ionized carbon dioxide molecules have been identified. By studying the covariance mapping mass spectroscopy of the electron impact ionization of CO_2 we have measured the absolute cross sections of the ion-pair dissociation channels in double, triple, and quadruple ionization of CO_2. The absolute cross sections of some channels involving neutral fragments are also derived. The experiment shows that the total cross section of single, double, and triple ionization decreases by at least an order of magnitude as the ionization increases by one stage.

By studying the structures of the islands in the covariance map, we have concluded that one of the ${CO_2}^{2+}$ dissociation channels ${CO_2}^{2+} \rightarrow C^+ + O^+ + O$ is dominated by the process of secondary decay. The channel ${CO_2}^{2+} \rightarrow 2O^+ + C$ is a concerted process, where the two O^+ ions fly apart simultaneously and with similar momentum. The three-body dissociation channels of triply ionized carbon dioxide are found to be dominated by concerted processes no matter how the charges are distributed on the fragments. The momentum distributions on the fragments in different channels have been obtained from the structure of the covariance map. The dissociation dynamics of triply ionized carbon dioxide is also studied. The momentum distribution can only be explained by the charge exchange model, where the electric charge is mobile when the distances between the fragments are not too large. The metastable decay of ${CO_2}^{2+}$ is also observed directly. Analysis shows that its covariance map is a velocity contour. The difference of electron impact ionization with respect to other excitation schemes such as photoionization, heavy ion impact, and high intensity laser field ionization is also discussed.

ACKNOWLEDGMENTS

One of the authors (C. T.) is grateful to the Alexander von Humboldt Foundation for the financial support for staying at the Max-Planck-Institute for Extraterrestrial Physics. The technical support of B. Steffes and stimulating discussions with T. Sykora are also appreciated.

[1] M. Larsson, Comments At. Mol. Phys. **29**, 39 (1993), and references therein.
[2] For example, W. T. Hill III, J. Zhu, D. L. Hatten, Y. Cui, J. Goldhar, and S. Yang, Phys. Rev. Lett. **69**, 2646 (1992).
[3] L. J. Frasinski, K. Codling, and P. A. Hatherly, Science **246**, 1029 (1989).
[4] G. Sampoll, R. L. Watson, O. Heber, V. Horvat, K. Wohrer, and M. Chabot, Phys. Rev. A **45**, 2903 (1992).
[5] D. Mathur, E. Krishnakumar, K. Nagesha, V. R. Marathe, V. Krishmurth, F. A. Rajgara, and U. T. Raheja, J. Phys. B **26**, L141 (1993).
[6] P. Lablanquie, J. Delwiche, M. -J. Hubin-Franskin, I. Nenner, P. Morin, K. Ito, J. H. D. Eland, J. -M. Robbe, G. Gandara, J. Fournier, and P. G. Fournier, Phys. Rev. A **40**, 5673 (1989).
[7] T. Masuoka E. Nakamura, Phys. Rev. A **48**, 4379 (1993).
[8] T. Masuoka, J. Chem. Phys. **101**, 322 (1994).
[9] T. Masuoka, E. Nakamura, and A. Hiraya, J. Chem. Phys. **104**, 6200 (1996).
[10] M. R. Bruce, L. Mi, C. R. Sporleder, and R. A. Bonham, J. Phys. B **27**, 5773 (1994).
[11] G. Speckowius and B. Brehm, Chem. Phys. Lett. **187**, 442 (1991).
[12] S. Hsieh and J. H. D. Eland, J. Chem. Phys. **103**, 1006 (1995).
[13] S. Hsieh and J. H. D. Eland, J. Phys. B **30**, 4515 (1997).
[14] T. Matsuo, T. Tonuma, M. Kase, T. Kambara, H. Kumagai, and H. Tawara, Chem. Phys. **121**, 93 (1988).

[15] G. Herzberg, *Molecular Spectra and Molecular Spectra* (Van Nostrand Reinhold Company, New York, 1966), Vol. III.
[16] C. E. Moore, *Atomic Energy Levels*, Natl. Bur. Stand. (U.S.) Circ. No. 467 (U.S. GPO, Washington, DC, 1949), Vol. I.
[17] Cechan Tian and C. R. Vidal, J. Chem. Phys. **108**, 927 (1998).
[18] Cechan Tian and C. R. Vidal, J. Phys. B **31**, 895 (1998).
[19] L. J. Frasinski, P. A. Hatherly, K. Codling, M. Larson, A. Persson, and C. -G. Wahlström, J. Phys. B **27**, L109 (1994).
[20] Goodfellow Inc.
[21] Hamamatsu Inc.
[22] C. Ma, M. R. Bruce, and R. A. Bonham, Phys. Rev. A **44**, 2921 (1991).
[23] B. Brehm, J. Grosser, T. Ruscheinski, and M. Zimmer, Meas. Sci. Technol. **6**, 953 (1995).
[24] H. C. Straub, P. Renault, B. G. Lindsay, K. A. Smith, and R. F. Stebbings, Phys. Rev. A **52**, 1115 (1995).
[25] R. Locht and M. Davister, Int. J. Mass Spectrom. Ion Processes **144**, 105 (1995).
[26] H. Hogreve, J. Phys. B **28**, L263 (1995).
[27] Th. A. Field, and J. H. D. Eland, Chem. Phys. Lett. **211**, 436 (1993).
[28] T. Masuoka, Phys. Rev. A **50**, 3886 (1994).
[29] M. Schmidt, D. Normand, and C. Cornaggia, Phys. Rev. A **50**, 5037 (1994).
[30] L. J. Frasinski, A. J. Giles, P. A. Hatherly, J. H. Posthumus, M. R. Thompson, and K. Codling, J. Electron Spectrosc. Relat. Phenom. **79**, 367 (1996).